A&A 502, 341–344 (2009)
DOI: 10.1051/0004-6361/200811494

Astronomy & Astrophysics

Electron acceleration in the turbulent reconnecting current sheets in solar flares *(Research Note)*

G. P. Wu[1] and G. L. Huang[2]

[1] Department of Physics, Southeast University, Nanjing, Jiangsu 210096, PR China
e-mail: wuguiping@seu.edu.cn
[2] Purple Mountain Observatory, Chinese Academy of Sciences, Nanjing, Jiangsu 210008,PR China

Received 10 December 2008 / Accepted 28 April 2009

ABSTRACT

Context. We investigate the nonlinear evolution of the electron distribution in the presence of the strong inductive electric field in the reconnecting current sheets (RCS) of solar flares.
Aims. We aim to study the characteristics of nonthermal electron-beam plasma instability and its influence on electron acceleration in RCS.
Methods. Including the external inductive field, the one-dimensional Vlasov simulation is performed with a realistic mass ratio for the first time.
Results. Our principal findings are as follows: 1) the Buneman instability can be quickly excited on the timescale of 10^{-7} s for the typical parameters of solar flares. After saturation, the beam-plasma instabilities are excited due to the non-Maxwellian electron distribution; 2) the final velocity of the electrons trapped by these waves is of the same order as the phase speed of the waves, while the untrapped electrons continue to be accelerated; 3) the inferred anomalous resistance of the current sheet and the energy conversion rate are basically of the same order as those previously estimated, e.g., "the analysis of Martens".
Conclusions. The Buneman instability is excited on the timescale of 10^{-7} s and the wave-particle resonant interaction limits the low-energy electrons to be further accelerated in RCS.

Key words. turbulence – Sun: magnetic fields – acceleration of particles

1. Introduction

In solar flares, the nonthermal electrons often contain about 10–50% of the total released energy (Lin & Hudson 1976; Dennis et al. 2003; Lin et al. 2003). These electrons generate the observed hard X-ray (HXR) bremsstrahlung as they lose most of their energy by coulomb collisions in the lower corona and chromosphere. Their distribution inferred from HXR emission is well described by a power law with a low-energy cutoff in the range of 20–40 keV (Brown 1971; Dennis 1985; Benka & Holman 1994; Holman 2003; Miller et al. 1997; Aschwanden 2002; Sui et al. 2004). The total HXR flux has been found to exhibit a temporal correlation with both the HXR source separation speed and the reconnection rate, i.e., the induced electric field strength. It may be calculated from the flare ribbon separation speed and the photosphere magnetic field, and may reach about 1–10 V cm^{-1} (Poletto & Kopp 1986; Lin et al. 2003; Forbes & Lin 2000; Qiu et al. 2002; Jing et al. 2005).

In the externally driven reconnecting current sheet (RCS), numerous theoretical investigations have been devoted to the study of electron acceleration in the presence of super-Dreicer electric field in solar flares, using test particle simulations (Speiser 1965; Martens & Young 1990; Litvinenko 1996, 2003; Onofri et al. 2006; Petkaki & MacKinnon 2007; Dauphin et al. 2007), as reviewed by Miller et al. (1997) and Aschwanden (2002). With a prescribed induced electric field and three-dimensional (3D) magnetic configuration but without wave-particle interactions, the equation of motion for a single particle was solved (Litvinenko 1996; Heerikhuisen et al. 2002). It was found that the most efficient acceleration took place inside the diffusion region with a guiding magnetic field, the energetic electrons appear on a power-law distribution, and the spectral index depends mainly on the magnetic configuration (Litvinenko 2000). The development of the 2D particle-in-cell (PIC) simulations confirmed that the relativistic electrons are mainly accelerated inside the diffusive region with the large guiding magnetic field component (Pritchett 2006). Furthermore, up to ∼300 keV electrons were directly measured in a rare crossing of the diffusion region of Earth's magnetotail by the Wind spacecraft (Øieroset et al. 2002).

Omura et al. (2003) considered that such a magnetic configuration and a 1D approach may be enough to study the plasma response to a strong parallel electric field along the guide field lines, and performed a 1D PIC simulation with typical parameters for the magnetopause. Since the drift velocity of electrons relative to ions is larger than the threshold of Buneman instability for a similar electron and ion temperature (Buneman 1959), the electrostatic wave was quickly excited. After the saturation of the unstable waves, the maximum strength of the turbulent electric field is about two orders of magnitude larger than the applied induced field. The pioneering 1D PIC simulation with reduced mass ratio and small particles provided similar results in the presence of quite strong electric field (Boris et al. 1970). In their 3D self-consistent PIC simulations of two current sheet reconnection, Drake et al. (2003) demonstrated that the electrons are accelerated near the magnetic x-line and separatrices, then,

these electron beams excite the Buneman instability, and finally, the intense electric fields scatter and energize the electron beams. All of these steps imply that wave-particle interactions should be considered in the investigation of electron acceleration in externally driven RCS in solar flares.

We solved the linear dispersion relation of 1D drift Maxwellian distributions of electrons and protons with the typical parameters in solar corona (Wu et al. 2008), and obtained some preliminary results, such as the low frequency waves are excited on the timescale of 10^{-7} s, the trapped electrons by these waves stopped being accelerated, and the nonthermal electrons appear to have a double power-law distribution. These results need to be verified. In this paper, the nonlinear evolution of instability is solved in the 1D Vlasov equation with externally driven electric field for the first time in solar flares, for studying its effect on the electron acceleration. The basic equation and simulation method are presented in Sect. 2. The dispersion and evolution in the unstable waves are described in Sect. 3. The conclusions and discussions are given in Sect. 4.

2. Basic equation and simulation method

Boris et al. (1970) performed one and two dimensional PIC simulations in the presence of a very strong electric field along the x-axis of an electron-positron plasma, and found that only waves parallel to electric field are strongly excited (in 2D simulations), the increase in velocity in y direction being very small. They concluded that one-dimensionality may not be a serious limitation. Therefore, a 1D approach is adopted in this paper to investigate the electron acceleration in RCS.

There are two assumptions adopted in this paper: 1) $B_x \approx B_y \approx 0$, which are appropriate in the center-plane of a current sheet near the X-type point, where the electrons are most effectively accelerated (Coroniti and Eviatar 1977; Pritchett 2006; Øieroset et al. 2002); 2) the Lorentz force ($\boldsymbol{J}\times\boldsymbol{B}$) is smaller than the electric force, when the induced electric field is assumed to be along the z-component of the magnetic field (Omura et al. 2003).

However, these assumptions are theoretical, and can not be directly inferred from observations of the solar corona (Watt et al. 2002; Petkaki & Freeman 2008). Therefore, for the study of electrostatic waves, the only force acting on the plasma is that of an electric field, and the 1D electrostatic Vlasov equation is written as (Petkaki & Freeman 2008)

$$\frac{\partial f_\alpha}{\partial t} + v_z\frac{\partial f_\alpha}{\partial z} + \frac{q_\alpha}{m_\alpha}E_z\frac{\partial f_\alpha}{\partial v_z} = 0, \tag{1}$$

where f_α is the particle distribution function ($\alpha \in \{\mathrm{i},\ \mathrm{e}\}$), m_α and q_α are respectively the mass and charge of particles, and E_z is the electric field strength, including the inductive component E_0 and turbulent component $\widehat{E}$, i.e., $E_z = E_0 + \widehat{E}$. The former is assumed to be a constant in time and space, and the latter may be integrated forward in time, using Ampere's law given by

$$(\nabla\times\boldsymbol{B})_z = \mu_0\left(J + \varepsilon_0\frac{\partial E_z}{\partial t}\right). \tag{2}$$

The electric current density is expressed by

$$J(z,t) = \sum q_\alpha \int v_z f_\alpha(z, v_z, t)\mathrm{d}v_z, \tag{3}$$

which may also be divided into two parts of the spatially-averaged component and the fluctuant component, the former being assumed to be balanced by the gradient of an external magnetic field $\boldsymbol{B}$ at all time, i.e., $(\nabla\times\boldsymbol{B})_z = \mu_0\langle J\rangle$ (Omura et al. 1996; Watt et al. 2002), and the latter being related to the turbulent electric field, which is given by $\widehat{J} = J - \langle J\rangle$.

Table 1. Summary of simulation parameters.

Parameters	Symbol	Value
Ion to electron mass ratio	$m_\mathrm{p}/m_\mathrm{e}$	1836
Plasma density	$n = n_\mathrm{i} = n_\mathrm{e}$	10^{14} m^{-3}
Temperature	$T = T_\mathrm{e} = T_\mathrm{i}$	10^7 k
Initial drift velocity	v_d	$1.4v_{\mathrm{e}0}$
Number of space grid points	N_z	2000
Number of velocity grid points	$N_{\mathrm{ve}}, N_{\mathrm{vi}}$	2500, 400
Resolution of spacial grid	Δz	$0.5\lambda_\mathrm{De}$
Resolution of velocity grid	$\Delta v_\mathrm{e}, \Delta v_\mathrm{i}$	$0.01v_{\mathrm{e}0}, 0.05v_\mathrm{i}$
Resolution of time	Δt	$0.003w_\mathrm{pe}^{-1}$

The anomalous resistivity may be calculated using the following expression:

$$\eta_\mathrm{eff} = \frac{E_0}{\langle J\rangle} - \frac{m_\mathrm{e}}{n_\mathrm{e}\mathrm{e}^2}\left(\frac{1}{\langle J\rangle}\frac{\mathrm{d}\langle J\rangle}{\mathrm{d}t}\right). \tag{4}$$

With the periodic boundary conditions and simulation method described in Horne & Freeman (2001), Eq. (1) is integrated forward in time. The initial unstable waves originate in a white noise electric field applied at $t = 0$ (see Eqs. (4) and (5) in Petkaki et al. 2003). The simulation parameters are summed in Table 1, where n, T are respectively the plasma density and temperature, $v_\mathrm{d}, v_{\mathrm{e}0}$, and v_i are respectively the initial bulk drift velocity, electron, and proton thermal velocity ($v_{\mathrm{e}0} = \sqrt{kT/m_\mathrm{e}}, v_\mathrm{i} = \sqrt{kT/m_\mathrm{i}}$, k is the Boltzmann constant, m_e is the electron mass, m_i is the proton mass), and $\lambda_\mathrm{De}, \omega_\mathrm{pe}$ are the plasma Debye length and electron plasma frequency, respectively. The space, velocity space, and time numbers of grid points are carefully selected to ensure the numeric stability and accuracy of the integration algorithm (Horne & Freeman 2001; Petkaki et al. 2003).

To verify our results, we used the same parameters as used in Fig. 3 of Watt et al. (2002), and found similar evolution in the distribution function and the turbulent wave energy. When the inductive field added, the results comparable with the PIC simulation with the same parameters as those used in Omura et al. (2003). We also find similar result for the evolution in the unstable wave energy and the bulk drift velocity as shown in Fig. 2 of Omura et al. (2003).

3. Simulation results

3.1. Evolution in the electron distribution

The electron distribution at $z = 0$ for $\omega_\mathrm{pe}t = 90$, 240, and 600 are shown in Figs. 1a–c respectively for $E_0 = 500$ V m^{-1}. Figure 1d shows the evolution in the spatially averaged density of the turbulent energy versus time, where $\sigma_\mathrm{E} = \frac{\varepsilon_0\widehat{E}^2}{2n_\mathrm{e}kT}$. The spatially averaged mean drift velocity, thermal velocity, free accelerated velocity of electrons, and the anomalous resistivity versus time with different magnitudes of external inductive fields are shown in Fig. 2. It is shown from Figs. 1 and 2 that the whole evolution can be divided into three stages. At the beginning, the electrons are all accelerated by the induced electric field, and Buneman instability is excited. Then the unstable waves increase exponentially. With the increase in the magnitude of unstable waves, the kinetic energy of electrons is transferred into waves, and the drift velocity decreases. Some electrons are

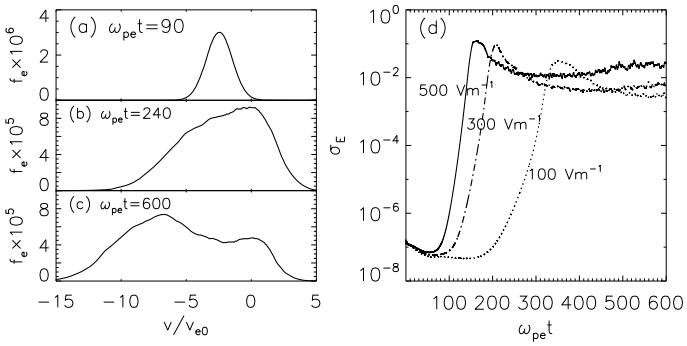

Fig. 1. Evolution in the electron distribution with inductive field strength of 500 V m^{-1} in **a)–c)**, and the fluctuating electric field energy with different inductive field strength **d)**.

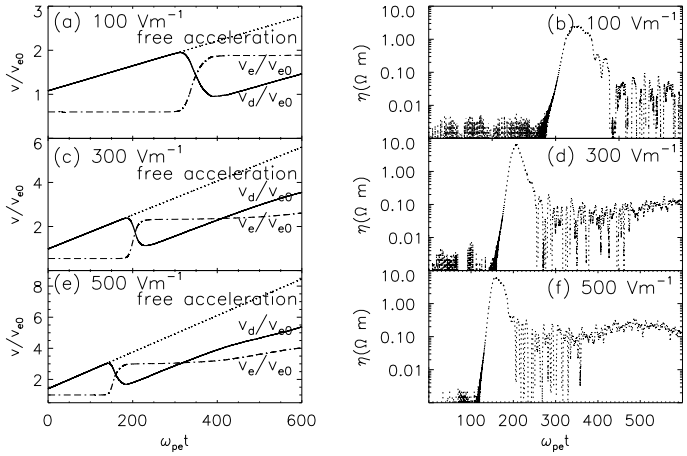

Fig. 2. Evolution in bulk drift velocity, thermal velocity, and free accelerated velocity of electrons in **a)**, **c)**, **e)**, and the anomalous resistivity in **b)**, **d)**, and **f)** for three different induced electric fields.

trapped in waves by Landau damping, a low-velocity tail appears relative to the distributions in Figs. 1a and c, and their acceleration stops. At this stage, the perturbed energy may be expressed by $\sigma_E \propto e^{2\gamma t}$, where γ is the growth rate. When the unstable wave energy increases from 10^{-5} to 10^{-3}, γ equals respectively about 4.95 ω_{pi}, 3.96 ω_{pi}, and 2.6 ω_{pi}, i.e., 6.5×10^7 s^{-1}, 5.2×10^7 s^{-1}, and 3.4×10^7 s^{-1} for the different inductive fields of 500 V m^{-1}, 300 V m^{-1}, and 100 V m^{-1}, where ω_{pi} is the ion plasma frequency. These results are consistent with our previous solutions of the linear dispersion relation that the growth rate depends strongly on the drift velocity (Wu et al. 2008). It means that the unstable waves can be excited within a typical acceleration timescale of 10^{-6} s (Litvinenko 1996; Wu et al. 2005). Finally, instability saturates, untrapped electrons continue to be accelerated, and the bulk drift velocity continues to rise.

3.2. Anomalous resistivity

The anomalous resistivity inferred using Eq. (4) is shown in Figs. 2b, d, and f for different electric fields, while the Spitzer collisional resistivity η is 7×10^{-9} Ω m. It increases by at least a factor of about 10^6. The sheet resistance may be estimated to be $R_s = \frac{\eta_{eff}L}{4ab} \approx 0.01 \sim 1$ Ω in the saturate state, where the length L and the width b of the sheet are assumed to be the same as those taken by Martens (1988), and the thickness of the sheet is $a = 1$ m. Taking the sheet current intensity to be $10^{11} \sim 10^{12}$ A,

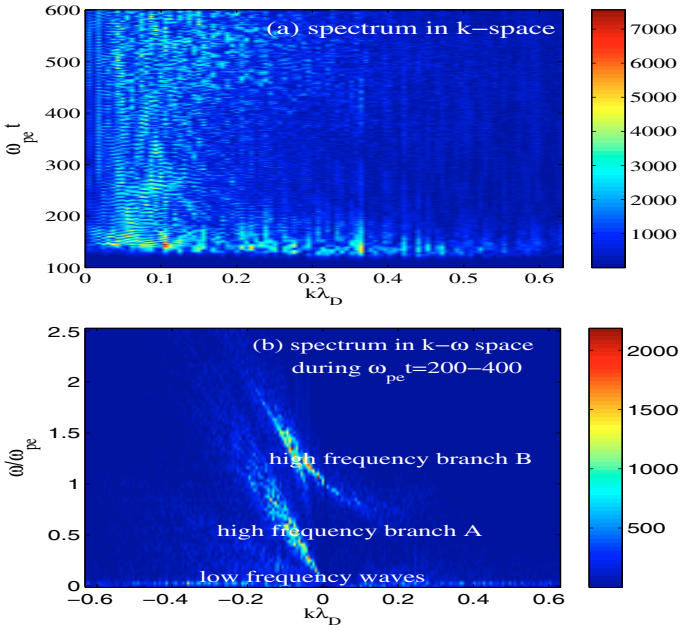

Fig. 3. Turbulent electric field spectra obtained by Fourier transformation with the induced electric field of 500 V m^{-1}.

the energy conversion rate is about $10^{27} \sim 10^{31}$ erg s^{-1}, and is enough to interpret the energy conversion and fast magnetic reconnection in the impulsive phase of solar flares (Martens 1988).

3.3. Dispersion of unstable waves

For the sake of analyzing further the nonlinear characteristics of unstable electrostatic waves, a 2D Fourier transformation to turbulent electric field was performed, for which spectra in k-t and in k-ω space are shown respectively in Fig. 3. This figure shows that the wave number of maximum growth waves decreases with the increase in average bulk drift velocity during the time interval of $\omega_{pe}t = 120-180$, the low-frequency waves are excited and propagate in opposite directions, which is the typical property of Buneman instability (Buneman 1959). By means of the Landau damping, the low-speed electrons appear in velocity space (see Figs. 1a to c). Then, because of the deviation of the electron distribution from Maxwellian one, the beam-plasma instabilities are excited (Hamberger & Jancraik 1972). The two new unstable wave branches (A, B in Fig. 3b) appear: one is located in the frequency domain of (0.1–0.8) ω_{pe} in phase velocity of about several times their initial thermal velocity, the other is located in the frequency domain of (1–1.5) ω_{pe} with a phase velocity of about dozen times their initial thermal velocity. With the excitation of high frequency waves, the strength of low frequency waves is lower than that of high frequency waves. To understand why these waves are excited, we solve the dispersion equation of double components of electrons that move at different velocities relative to ions in the cold plasma approximation given by

$$1 - \frac{\omega_{pi}^2}{\omega^2} - \frac{\alpha_1\omega_{pe}^2}{(\omega - ku_1)^2} - \frac{\alpha_2\omega_{pe}^2}{(\omega - ku_2)^2} = 0, \quad (5)$$

where α_1 and α_2 are the density ratio of each component, u_1 and u_2 are the respective drift velocities of each component. Assuming α_1, α_2, u_1, and u_2 respectively equal 0.95, 0.05, $6v_{e0}$, and $1.5v_{e0}$, the two unstable waves are found in Fig. 4. The low-frequency wave corresponds to Buneman instability, the

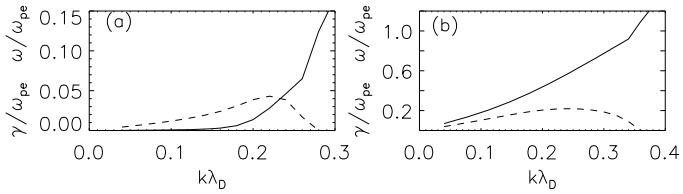

Fig. 4. Frequency ω (Solid line) and the growth rate γ (dashed line) of unstable waves versus wave-number, for a **a)** a low-frequency branch; **b)** a high-frequency branch.

high-frequency wave may correspond to the branch A shown in Fig. 3b. If more components are added, there may be more unstable waves. These results are consistent with the early toroidal anomalous resistivity experiment on the evolution of multi-electrons accelerated by a parallel electric field, in which the electron distribution acquires two components, one moving much faster than the other, the beam-plasma instability is excited, and the spectrum of unstable waves may begin about ω_{pi} and extend beyond ω_{pe} (Richardson et al. 1978).

4. Conclusions and discussions

In principle, the particle acceleration may be fully understood only when the 3D self-consistent dynamic reconnection is solved. However, because of the practical limit to the run time and storage memory of computers, a simplified model and unrealistic plasma parameters are often used to obtain some insight into the physical nature (Pritchett 2006; Wu et al. 2005). In space science, 1D Vlasov simulation has been used to study the ion-acoustic instability of the initial drift Maxwellian or non-Maxwellian distribution in the magnetopause. It has been found that the anomalous resistivity in saturation state depends on reduced mass ratio, and increases with the enhancement of the mean drift velocity (Watt et al. 2002; Petkaki et al. 2003, 2006). In 2D PIC simulations, Pritchett (2006) discovered that the most efficient electron acceleration in RCS takes place near the X-line of the externally driven RCS with a guiding magnetic field. Omura et al. (2003) performed 1D PIC simulations of the plasma response to an applied electric field parallel to magnetic field lines, found that the Buneman instability is excited, and that the amplitude of the unstable wave is about two orders of magnitude larger than the applied induced field in the magnetopause. In solar physics, test particle simulations have been extensively used in almost all studies of particle acceleration without taking the effect of turbulent waves into account (Martens & Young 1990; Litvinenko 1996, 2003; Onofri et al. 2006). Using a 1D Vlasov simulation and including the inductive electric field with a realistic mass ratio for the first time, we have illustrated the excitation of unstable waves and their influences on the acceleration of electrons along the guiding magnetic field that have the typical parameters of solar flares. The main results are summarized as follows.

At first, owing to the presence of a super-Dreicer electric field, the bulk drift velocity increases beyond the threshold of Buneman instability on the timescale of 10^{-7} s, and Buneman instability can be quickly excited compared with the typical acceleration time of 10^{-6} s. Wave-particle Landau damping then causes the low-velocity tail to be formed. Finally, the more unstable waves appear because of the deviation of the electron distribution from a Maxwellian one, which is also proven by the analytical calculation of the dispersion relation including two component electrons of different drift velocity in the cold plasma approximation.

We have self-consistently evaluated the anomalous resistivity, which enhances the classical resistivity by at least 10^6 orders of the magnitude in the saturating state. Its value is the same order as the one inferred from energy conversion in solar flares (Martens 1988), and often adopted in most previous studies, such as magnetic reconnecting simulations.

We emphasize that the distribution of the energetic electrons in RCS could not be obtained by the present 1D simulation, because the small magnetic field component perpendicular to the guiding field is ignored, which causes the electrons to move outside the diffusion region without further acceleration. Only when 3D electromagnetic simulation in RCS is performed, can the self-consistent energetic electron spectrum be acquired.

Acknowledgements. We are grateful to the referee for constructively critical comment leading to significant improvement of the manuscript. This study is supported by the NFSC projects with Nos. 10773032, 10833007, and "973" program with No. 2006CB806302.

References

Aschwanden, M. J. 2002, Space Sci. Rev., 101, 1
Benka, S. G., & Holman, G. D. 1994, ApJ, 435, 469
Boris, J. P., Dawson, J. M., & Orens, J. H. 1970, Phys. Rev. Lett., 25, 706
Brown, J. C. 1971, Sol. Phys., 18, 489
Buneman, O. 1959, Phys. Rev. Lett., 115, 503
Coroniti, F. V., & Eviatar, A. 1977, ApJS, 33, 189
Dennis, B. R. 1985, Sol. Phys., 100, 465
Dennis, B. R., Veronig, A., Schwartz, R. A., et al. 2003, Adv. Space Res., 32, 2459
Drake, J. F., Swisdak, M., Cattell, C., et al. 2003, Science, 299, 873
Forbes, T. G., & Lin, J. 2000, J. Atmos. Sol.-Terr. Phys., 62, 1499
Hamberger, S. M., & Jancraik, J. 1972, Phy. Fluids, 15, 825
Heerikhuisen, J., Litvinenko, Y. E., & Craig, I. J. D. 2002, ApJ, 566, 512
Holman, G. D. 2003, ApJ, 586, 606
Horne, R. B., & Freeman, M. P. 2001, J. Comp. Phys., 171,182
Jing, J., Qiu, J., Lin, J., et al. 2005, ApJ, 620, 1085
Lin, R. P., & Hudson, H. S. 1976, Sol. Phys., 50, 153
Lin, R. P., Krucker, S., Hurford, G. J., et al. 2003, ApJ, 595, L69
Litvinenko, Y. E. 1996, ApJ, 462, 997
Litvinenko, Y. E. 2000, Sol. Phys., 194, 327
Litvinenko, Y. E. 2003, Sol. Phys., 212, 379
Martens, P. C. H. 1988, ApJ, 330, L131
Martens, P. C. H., & Young, A. 1990, ApJS., 73, 333
Miller, J. A., Cargill, P. J., Emslie, A., et al. 1997, J. Geophys. Res., 102, 14631
Øieroset, M., Lin, R. P., Phan, T. D., Larson, D. E., & Bale, S. D. 2002, Phys. Rev. Lett., 89, 195001
Omura, Y., Matsumoto, H., Miyake, T., & Kojima, H. 1996, J. Geophys. Res., 101, 2685
Omura, Y., Heikkila, W. J., Umeda, T., Ninomiya, K., & Matsumoto, H. 2003, J. Geophys. Res., 108A(5), 1197
Onofri, M., Isliker, H. G. A., & Vlahos, L. 2006, Phys. Rev. Lett., 96, 151102
Petkaki, P., Watt, C. E. J., Horne, R. B., & Freeman, M. P. 2003, J. Geophys. Res., 108, 1442
Petkaki, P., Freeman, M. P., Kirk, T., Watt, C. E. J., & Horne, R. B. 2006, J. Geophys. Res., 111, 1205
Petkaki, P., & MacKinnon, A. L. 2007, A&A., 472, 623
Petkaki, P., & Freeman, M. P. 2008, ApJ, 686, 686
Poletto, G., & Kopp R A. 1986, in The Lower Atmosphere of Solar Flares,Proceedings of the Solar Maximum Mission Symposium, Sunspot, NM, Aug. 20–24 (A87-26201 10-92), 453
Pritchett, P. L. 2006, J. Geophys. Res., 111, A10212
Qiu, J., Lee, J., Gary, D. E., & Wang, H. 2002, ApJ, 565, 1335
Richardson, R., Gentle, K. W., & Leifeste, G. T. 1978, Phy. Fluids, 21, 1417
Speiser, T. W. 1965, J. Geophys. Res., 70, 8211
Sui, L. H., Holman, G. D., & Dennis, B. R. 2004, ApJ, 612, 546
Watt, C. E. J., Horne, R. B., & Freeman, M. P., 2002, Geophys. Res. Lett., 29, 1004
Wu, G. P., Huang, G. L., & Tang, Y. H. 2005, Chin. J. Astron. Astrophys., 5, 99
Wu, G. P., Huang, G. L., Huang, Y., & Wang, D. Y. 2008, Adv. Space Res., 41, 984